Accelerated Antarctic ice loss through ocean forced changes in subglacial hydrology

Sophia Pinter
University of California Santa Cruz
Gavin Piccione (gpiccion@ucsc.edu)
University of California Santa Cruz https://orcid.org/0000-0002-7637-9796
Terrence Blackburn
University of California Santa Cruz
Slawek Tulaczyk
University of California, Santa Cruz https://orcid.org/0000-0002-9711-4332

Article

Keywords:

Posted Date: February 1st, 2023

DOI: https://doi.org/10.21203/rs.3.rs-2464588/v1

Additional Declarations: There is **NO** Competing Interest.

Accelerated Antarctic ice loss through ocean forced changes in subglacial hydrology

Sophia Pinter[1], Gavin Piccione[1], Terrence Blackburn[1], Slawek Tulaczyk[1]*

University of California, Santa Cruz, Earth and Planetary Sciences, 1156 High Street, Santa Cruz, CA 95064, USA.

* Correspondence to: gpiccion@ucsc.edu

Abstract: Recent changes in Southern Ocean temperature have been linked with catchment-wide Antarctic ice acceleration and loss. The ice sheet models producing future sea level projections, however, rely on controversial mechanisms to match this rapid response, possibly due to the omission of feedbacks between subglacial water pressure and ice velocity. While modern remote sensing data tie increased subglacial water pressure to ice acceleration, there exists no record of subglacial hydrology long enough to evaluate this feedback on timescales relevant to climate and sea level change. Here we present a ten-thousand-year record of subglacial water dynamics and chemistry from ~110 ka East Antarctic calcite and sediment-bearing subglacial precipitates. Time series of sediment frequency and grain size indicate that changes in subglacial water dynamics correlate with Southern Ocean temperature. Similarly, shifts in calcite composition record climate-driven changes in subglacial water provenance. The synchronized changes in subglacial hydrology with climate support subglacial water drainage systems as having a key role in transferring the climate forcing acting on ice sheet margins, deep into ice sheet interior. The demonstrated coupling between subglacial water and climate clarifies the current rapid ice response to climate change in Antarctica, and underscores a need and means to heighten the sensitivity of ice sheet models.

Introduction:

Resolving the timescales over which ice sheets respond to climate change is a fundamental issue in current efforts to forecast the contribution of Antarctica to global sea level rise under various warming scenarios[1,2]. Pioneering work on advective, and diffusive glaciological response mechanisms indicated that within a polar ice sheet, climate-driven perturbations propagate several times faster than the ice flow velocity[3]. Given that the bulk of the Antarctic ice sheet (AIS) moves slowly[4], early numerical ice sheet models suggested that it may take up to several centuries for future climate warming to result in a significant contribution to sea level rise from Antarctica[5]. However, rapid changes observed within the AIS in the recent decades[6] do not appear to be consistent with such slow ice sheet response timescales, suggesting that some other glaciological mechanisms, such as the subglacial hydrologic system, may accelerate the response of ice sheets to climate change[7].

Remote sensing of the AIS has revealed a widespread subglacial hydrologic system consisting of saline groundwaters[8,9], lakes[10], and channels connecting subglacial water bodies over hundreds of kilometers[11,12]. This hydrologic system drains meltwater generated at the base of the ice sheet and is observed to respond to climate change on timescales of hours to years[2]. The physical reason for the short response timescale of basal hydrology as compared to the long response timescale of ice sheets is rooted in the fact that the dynamic viscosity of water is about fifteen orders of magnitude lower than the effective viscosity of glacier ice[13]. At the same time, subglacial water pressure controls the rate of ice sliding[14,15], leaving open the possibility that the inclusion of realistic subglacial water dynamics can make ice sheet response to climate change

significantly faster than suggested by analytical or numerical ice sheet models that disregard it[3,5]. Even the relatively short record of Antarctic instrumental observations covering the last few decades, yields several examples of significant ice flow accelerations induced by floods emanating from subglacial lake basins[16–18].

In a recent modeling paper, Dow and others hypothesized that climate-driven grounding line retreat results in increased ice surface slopes that amplify basal melting and subglacial water pressure, which ultimately lead to strong catchment-wide ice acceleration[19]. These hydrological feedbacks reinforce high ice velocities in outlet glaciers and increase the drainage of subglacial water towards grounding lines. The increased discharge of buoyant subglacial meltwaters at grounding lines enhances submarine ice melting and promotes further grounding line retreat[19]. Together, this hydrologic model[19] and remote sensing observations of the modern ice sheet[20] suggest that a positive feedback exists between grounding line retreat, ice acceleration, and increased subglacial water drainage. However, there is currently no geologic record of subglacial hydrologic activity that can demonstrate whether proxies for subglacial water dynamics correlate with climate records, as this proposed positive feedback would suggest.

Here we present a ~10kyr archive of subglacial hydrologic changes recorded in finely laminated subglacial calcite precipitates that formed within the David-Mawson Glacier system during the later stages of Marine Isotope Stage 5. High-resolution U-series age constraints paired with spectral analyses of sedimentary laminae and geochemical characterization of subglacial waters demonstrate that the periodicity of subglacial flushing events, the size of abundance of siliciclastic grains and the composition of waters all correlate with climate records that track the temperatures of the Southern Ocean. We interpret the changes in subglacial water velocity and provenance as a response to climate-driven grounding line migration. Our records support a model[19] in which the feedback between grounding-line retreat, ice acceleration and subglacial hydrologic dynamics represents an important mechanism for rapid and enhanced response of the ice sheet to climate forcing.

Results:

A 10kyr archive of subglacial flushing, water dynamics and compositional change is recorded by two finely laminated accumulations of detrital silicate grains and calcite, that formed within a subglacial cavity beneath the AIS. Both samples were collected from Reckling Moraine (RM), East Antarctica, a sublimating section of exhumed basal ice that has entrained mostly rocks from the Transantarctic Mountains and a small percentage of chemical precipitates that form in subglacial environments[21]. Ice velocities and exhumation timescales of basal ice in this area of the Transantarctic Mountains place the origination of the precipitates within 10 km of RM[22], within the hydrologic network lying up glacier within the Mawson glacier drainage. The Mawson glacial catchment extends from Dome C to the Southern Ocean, and contains numerous mapped subglacial lakes of varying size[10] (Fig. 1 inset).

The focus of this study is on two subglacial precipitates, which consist predominantly of micron-scale laminations of clay-rich calcite that alternate with clean, columnar calcite (Extended Data Fig. 1 and Extended Data Fig. 2a). Superimposed on these recurrent laminations are layers of concentrated microcrystalline calcite containing silt to sand-sized (<250 μm) silicate grains often clustering at the base of the clay-rich calcite layers (Extended Data Fig. 2a). The sand grains within these layers are well sorted and rounded, both hallmarks of fluvial transport and unlike the textures observed in ice deposits (Extended Data Fig. 2a). These clastic layers are observed to pinch-out laterally, fining in transition, indicating unidirectional water flow (Extended Data Fig.

2b). Similarly, unidirectional flow produces the observed oblique foliation in the distribution of microcrystalline calcite[23] (Extended Data Fig. 2c). Laminated couplets from RM record a hydrologic sequence similar to those recorded in cave deposits[24]: a high flow event can erode the previously deposited calcite, rounding euhedral crystals, which can be capped by layers of sand to silt sized particles within a microcrystalline calcite matrix (Extended Data Fig. 2d). A return to low flow produces columnar calcite that transitions from clay-rich to clean calcite (Extended Data Fig. 2). Each sedimentary layer is interpreted to represent a discrete flushing event, where water and sediment are delivered unidirectionally into the sample forming water body and is followed by a period of low water flow. The more frequent micron-scale layering of clay-rich to clean calcite represent smaller, more frequent flushing events, while the sand layers represent less frequent, higher energy flushing events.

To determine the timing over which these changes in sediment delivery or subglacial water chemistry occurred, we produced ^{234}U-^{230}Th dates on the calcite from 10 and 12 horizons in each sample respectively (Methods and Extended Data Table 1). These calcite precipitation dates place the formation of each sample to 107.5 to 115.2 ka and 106.7 to 114.2ka (during MIS5e). The ^{234}U-^{230}Th date and the stratigraphic position of each dated horizon is used to produce a stratigraphic age model for each sample using a Markov-Chain Monte Carlo approach[25] (Extended Data Fig. 3; Methods). This stratigraphic age model provides the basis with which to construct a time series of 1) the periodicity of sediment delivery (Fig. 2), 2) the abundance of sand grains (Fig. 3f) and 3) chemical or isotopic changes in calcite composition (Fig. 3c,d,e).

To construct a time series of the periodicity in sediment delivery for each sample we utilized an evolutionary FFT technique (Methods) which revealed two dominant, though time-variant frequencies that can be correlated to physical aspects of the samples (Fig. 2 and Extended Data Fig. 4). The micron-scale laminations of clay-rich and clean calcite are associated with a centennial-scale frequency (Fig 2a,c,e). This high frequency change in sediment volume is present throughout the entire ~10 ka record of both samples, however, a consistent, high-power periodicity is only identified at two discrete time intervals: 108.5-109 ka and 112-113 ka (Fig. 2a and Fig. 3g). The next significant frequency parsed by the FFT is 500-1000 year periodicity (Fig. 2a,e). This frequency is physically associated with a ~cm-thick cycles in the total volume of siliciclastic delivered to the water body the samples formed in (Fig. 2c, e and Extended Data Fig. 5). Recalling from above, that each sedimentary layer represents a discrete flushing event, we interpret this periodic record of sediment delivery as resulting from the cyclic flushing of subglacial lakes upstream, and thus a record of lake flushing within the Mawson Glacier catchment. Apparent changes in depositional energy, including variations in grain size and changes in the overall abundance of sediment are attributed to changes in the water velocity from the flushing of upstream lakes with different volumes. For example, the micron-scale cycles in silicate and microcrystalline calcite content are interpreted to represent the flush of relatively small bodies of water, while intercalated clean calcite represent the lower flow periods of lake filling. The ~100 year periodicity at the two distinct time intervals of 108.5-109 ka and 112-113 ka suggests that the lakes within this glacial catchment experienced a sustained increase in water supply during these time intervals. In addition to changes in frequency, we measured the abundance of sand sized grains (Methods). A time series of sand abundance (Fig. 3f) also displays two prominent peaks at 108.5-109 ka and 112-113 ka, consistent with the interpretation that these represented isolated time periods of increased water velocity.

The chemical precipitates that form in aqueous environments under the EAIS reflect the chemistry of waters from which they precipitate[22,26,27]. To characterize the precipitate parent

waters, we report calcite isotopic composition ($^{87}Sr/^{86}Sr$, $^{234}U/^{238}U_i$, $\delta^{18}O$, $\delta^{13}C$) (Fig. 3c,d and Extended Data Table 2) and elemental concentrations ([U]) (Fig 3e and Extended Data Figure 7) over the ~10ka formation interval. The composition and secular changes in chemistry are the same for each sample, suggesting that both samples form in the same body of water, despite different sand volumes and precipitation rates. Beginning with the absolute values, the $\delta^{18}O_{SMOW}$ (-54-55 ‰, assuming T= 0 °C); Extended Data Table 2) of the waters from which the calcite precipitates are highly depleted in ^{18}O, up to 10 ‰ lighter than the ice found at RM. Yet, because the sample sizes and local ice velocities place the lake in which these samples form close to RM, these ^{18}O compositions require that waters have migrated from the headwaters of Mawson Glacier into lakes more proximal to RM (Fig. 1). The radiogenic $^{87}Sr/^{86}Sr$ compositions (>0.71), depart from meteoric glacial ice (~0.709) and indicate that these waters have chemically weathered silicate rocks during rock-water contact[28] (Fig. 3c). Similarly, the [$^{234}U/^{238}U$] (>2.6) composition of subglacial waters, are enriched in ^{234}U beyond melted glacial ice (~1.14 [29]) (Fig. 3d), which occurs through the alpha-injection of ^{234}U sourced from ^{238}U in silicate rock, also indicating long term physical contact between subglacial waters and silicate rocks[30]. Calcite U concentration can be controlled by the U concentration of the water[23] and thus the degree of rock-water interaction.

The elemental and isotopic composition of the calcite-forming subglacial waters change over the ~10 ka time interval. Long term trends include a decrease in $^{87}Sr/^{86}Sr$, U concentrations and [$^{234}U/^{238}U$]. Superimposed on this long-term record geochemical trend are two peaks, particularly well resolved by the higher fidelity $^{87}Sr/^{86}Sr$ and [U] time series at 108.5-109 ka and 112-113 ka (Fig.3). During these time intervals, the calcite forming waters exhibit both the highest values in $^{87}Sr/^{86}Sr$, $^{234}U/^{238}U$ and [U] as well as the highest variability in these values. The high $^{87}Sr/^{86}Sr$, [$^{234}U/^{238}U$] composition is indicative of prolonged rock water contact. Outside of these time intervals, the compositions are both less variable, and exhibit lower values of $^{87}Sr/^{86}Sr$, [$^{234}U/^{238}U$], and [U] (Fig.3).

Discussion:

The sedimentary and geochemical time series collected from the RM samples show that the dynamics and provenance of subglacial waters varied in concert with two short but prominent warming periods at 108.5-109 ka and 112-113. To examine the relationship between millennial-scale climate variations and the response of subglacial hydrology recorded in precipitate samples we compare the sample time series with the δD at EPICA Dome C (Fig. 3a), a paleotemperature proxy that is positively correlated with the temperature of the Southern Ocean abutting Antarctica[31]. The two peaks resolved in the sediment and geochemical data mimic the EDC climate record, aligning with millennial-scale Southern hemisphere warm periods known as Antarctic Isotopic Maximum or AIMs (Fig. 3). These short lived, AIM warm periods are driven by combined suppression of northward heat transport by Atlantic Meridional Overturning Circulation[32] (AMOC) and the upwelling of warm Southern ocean deep waters induced from southward shifts in southern hemisphere westerlies[33]. During MIS 5d, the strong and stable nature of AMOC[34] leads to relatively small millennial scale temperature changes (yellow dashed line, Fig 3a). However, the AIMS are readily identified by: 1) their temporal association with two Dansgaard-Oeschger (D-O) events (at ~109 and ~113 ka) in Greenland temperature records (purple, Fig. 3b) which consistently occur throughout the late Pleistocene within 300 years of peak AIM warming[35]; and 2) a decomposed record of AIM events in reference to the LR04 marine record[36] (solid yellow line, Fig. 3b).

The sedimentological and geochemical data proxies for subglacial water dynamics and provenance collected from RM samples, show a response that aligns with the AIM periods. For example, both the abundance of sand and an increase in the frequency of subglacial flooding occur during these warm periods implying that a greater volume of water contributes to a higher water energy and more frequent filling and flushing of subglacial lakes (Fig. 3f, g). In parallel, the composition of waters shifts during AIMS towards higher $^{87}Sr/^{86}Sr$ and [$^{234}U/^{238}U$] (Fig. 3c, d), indicating the introduction of waters that experienced longer timescales of water-rock interactions. We interpret this shift to more geochemically evolved waters during warm AIMs as resulting from a regional increase in hydrological connectivity which enables increased addition of more interior subglacial waters (e.g., from Wilkes subglacial lakes[10]). Estimates of the lag time between the sample data (constrained by the highest probability age model) and climate records place the peaks in hydrologic response to within 60 years of peak AIM warming (Extended Data Fig. 6), indicating a rapid response between subglacial water and ice velocity during the last interglacial just as demonstrated by modern measurements[16–18], and demonstrating a similar coupling to changes in ocean temperature.

Collectively, we interpret the coincidence of variations in water dynamics and provenance with millennial scale changes in climate as supporting the conceptual model for a key role of subglacial hydrology in enhancing climate sensitivity of marine-terminating Antarctic outlet glaciers[19]. Within the framework of this model, as illustrated in figure 4, the warming of ocean waters abutting the AIS during a warm period, leads to submarine ice melting and the retreat of grounding lines. This grounding line movement leads to a steepening of ice surface slopes, causing ice velocities to accelerate and the volume of subglacial waters to increase due to basal shear heating. This increase in water dynamics results in shortening of the fill-flush cycles of subglacial lakes and in the regional increase of subglacial water fluxes, which in a distributed subglacial drainage system is expected to increase water pressures and trigger faster ice flow. Furthermore, when increased subglacial water fluxes reach the grounding lines they can promote their continued retreat because they represent a significant buoyance flux that promotes vertical seawater mixing, enhanced vertical heat and salt transfer, and increased melting at the ice-ocean interface[19].

While ocean thermal forcing is invoked to explain grounding line retreat and ice acceleration in modern ice systems[6,37], the RM precipitate record reflects a new understanding of how warm ocean waters can drive changes in water pressure, and presumably with it ice acceleration, propagating deep into the ice sheet interior where large glacial and chemically mature waters reside[38] (e.g. Wilkes lake district, Fig. 1). In total, the analyzed subglacial archive supports the existence of rapidly responding positive feedback whereby Southern Ocean warming increases ice velocity, subglacial water supply, connectivity, and pressure, all of which feed back into higher ice velocities and may also promote further grounding line retreat due to the enhanced buoyancy fluxes and ice melting at the grounding line (Fig. 4c). The demonstrated connection between subglacial water and climate suggests that the feedbacks outlined here play a fundamental role in how ice sheets respond rapidly to climate change, both in the modern and the past, and underscores how the inclusion of these processes can improve the predictive power of ice sheet models.

METHODS

Subglacial Precipitate U-series age models

Geochronologic analyses were made on ~1 mm thick sections of each subglacial precipitate sampled parallel to calcite layers (Extended Data Fig. 1). U-series measurements were made at the W.M. Keck Isotope laboratory at UCSC following the methods described in ref. [27]. To construct the stratigraphic age model for each sample, we input sample height and ^{234}U-^{230}Th dates into a Bayesian Markov chain Monte

Carlo model that considers the age of each layer and its stratigraphic position within the sample to refine the uncertainty of each date using a prior distribution based on the principal of superposition[25]. Sample PRR53557 produced a more precise age-depth model than sample PRR52588, due to higher precipitation rates per unit time. Therefore, we use the age parameters from sample PRR53557 to produce a revised age-depth model for sample PRR52588 using a Monte Carlo simulation that finds the optimal time constraints, within dating uncertainties from PRR52588, to match the precipitate mineral line spectra from the two samples. This Monte Carlo simulation assumes, based on visual analyses of the mineral line spectra from the samples, that these two precipitates formed over the same time periods and that their calcite spectra should match through time. We choose tie points between the two samples where z-positions in PRR52588 match time constraints from PRR53557. We then run simulations for 10,000 age-depth models, within the 2σ uncertainty of the PRR52588 age constraints, and choose the age model that produces the most optimal match in line spectra between the two samples.

Spectral Analyses

To explore the timing and cyclicity of sample layers, we produced timeseries describing the amount of silicate detritus across each layer within the two subglacial precipitates. Spectra were produced by imaging the samples; converting the images to grey-scale to increase contrast of detritus; and using the image processing software, Fiji, to produce spectral outputs from box scans of grey-scale image transects (Fig. 2b,d). We used box scans to account for slight lateral variation of detritus within layers. Timeseries were produced by plotting these spectra versus age-depth models. We analyzed these timeseries for dominant frequency using the Fast Fourier Transform method of the Evolutionary Spectral Analysis feature in the program Acycle[39] (Fig. 2a). FFT measurements were determined using sliding windows with a width ~1.5x the size of the largest observed frequency in our spectra. Dominant frequencies were visualized as deconstructed spectra using the Signal Multiresolution Analyzer app in Matlab (Fig. 2e).

Delivery of sand-sized grains to the subglacial precipitates through time (Fig. 3f) was assessed using Scanning Electron Microscope- Energy Dispersive X-ray Spectroscopy (SEM-EDS) elemental images. Elemental maps showing calcium and silicon concentration were produced using EDS measured on a Thermoscientific Apreo SEM housed at UCSC. EDS data were generated using an Oxford Instruments UltimMax detector and were reduced using AZtecLive software. Abundance of sand-sized grains was quantified using Fiji software.

Isotopic measurements

Sr isotopic measurements were made at the UCSC Keck Isotope Laboratory following protocols outlined in ref. [27]. Carbonate isotope ratios ($\delta^{13}C_{CO3}$ and $\delta^{18}O_{CO3}$) were measured by UCSC Stable Isotope Laboratory using a Themo Scientific Kiel IV carbonate device and MAT 253 isotope ratio mass spectrometer. Referencing $\delta^{13}C_{CO3}$ and $\delta^{18}O_{CO3}$ to Vienna PeeDee Belemnite (VPDB) is calculated by two-point correction to externally calibrated Carrara Marble 'CM12' and carbonatite NBS-18[40]. Externally calibrated coral 'Atlantis II'[41] was measured for independent quality control. Typical reproducibility of replicates was significantly better than 0.05 ‰ for $\delta^{13}C_{CO3}$ and 0.1 ‰ for $\delta^{18}O_{CO3}$.

LA ICP-MS

Laser ablation inductively coupled plasma–mass spectrometry (LA ICP-MS) analyses were conducted at the Facility for Isotope Research and Student Training (FIRST) at Stony Brook University, following protocols outlined in ref. [22].

REFERENCES

1. Ritz, C. *et al.* Potential sea-level rise from Antarctic ice-sheet instability constrained by

observations. *Nature* **528**, 115–118 (2015).
2. Noble, T. L. *et al.* The sensitivity of the Antarctic Ice Sheet to a changing climate: Past, present and future. *Rev. Geophys.* 1–89 (2020). doi:10.1029/2019rg000663
3. Nye, J. F. The response of glaciers and ice-sheets to seasonal and climatic changes. *Proc. R. Soc. London. Ser. A. Math. Phys. Sci.* **256**, 559–584 (1960).
4. Bamber, J. L., Vaughan, D. G. & Joughin, I. Widespread complex flow in the interior of the antarctic ice sheet. *Science (80-.).* **287**, 1248–1250 (2000).
5. Huybrechts, P. & De Wolde, J. The dynamic response of the Greenland and Antarctic ice sheets to multiple-century climatic warming. *J. Clim.* **12**, 2169–2188 (1999).
6. Rignot, E., Mouginot, J., Morlighem, M., Seroussi, H. & Scheuchl, B. Widespread, rapid grounding line retreat of Pine Island, Thwaites, Smith, and Kohler glaciers, West Antarctica, from 1992 to 2011. *Geophys. Res. Lett.* **41**, 3502–3509 (2014).
7. Alley, R. B., Clark, P. U., Huybrechts, P. & Joughin, I. Ice-Sheet and Sea-Level Changes. *Science (80-.).* **310**, 456–461 (2005).
8. Foley, N. *et al.* Evidence for pathways of concentrated submarine groundwater discharge in east Antarctica from helicopter-borne electrical resistivity measurements. *Hydrology* **6**, (2019).
9. Toner, J. D., Catling, D. C. & Sletten, R. S. The geochemistry of Don Juan Pond: Evidence for a deep groundwater flow system in Wright Valley, Antarctica. *Earth Planet. Sci. Lett.* **474**, 190–197 (2017).
10. Wright, A. & Siegert, M. A fourth inventory of Antarctic subglacial lakes. *Antarct. Sci.* **24**, 659–664 (2012).
11. Wright, A. P. *et al.* Evidence of a hydrological connection between the ice divide and ice sheet margin in the Aurora Subglacial Basin, East Antarctica. *J. Geophys. Res. Earth Surf.* **117**, 1–15 (2012).
12. Wright, A. P. *et al.* Subglacial hydrological connectivity within the Byrd Glacier catchment, East Antarctica. *J. Glaciol.* **60**, 345–352 (2014).
13. Fowler, A. C. Glaciers and ice sheets. in *The Mathematics of Models for Climatology and Environment* (ed. Díaz, J. I.) 301–336 (Springer Berlin Heidelberg, 1997).
14. Iverson, N. R. Coupling between a glacier and a soft bed: II. Model results. *J. Glaciol.* **45**, 41–53 (1999).
15. Fowler, A. C. Weertman, Lliboutry and the development of sliding theory. *J. Glaciol.* **56**, 965–972 (2010).
16. Stearns, L. A., Smith, B. E. & Hamilton, G. S. Increased flow speed on a large east antarctic outlet glacier caused by subglacial floods. *Nat. Geosci.* **1**, 827–831 (2008).
17. Scambos, T. A., Berthier, E. & Shuman, C. A. The triggering of subglacial lake drainage during rapid glacier drawdown: Crane Glacier, Antarctic Peninsula. *Ann. Glaciol.* **52**, 74–82 (2011).
18. Siegfried, M. R., Fricker, H. A., Carter, S. P. & Tulaczyk, S. Episodic ice velocity fluctuations triggered by a subglacial flood in West Antarctica. *Geophys. Res. Lett.* **43**, 2640–2648 (2016).
19. Dow, C. F., Ross, N., Jeofry, H., Siu, K. & Siegert, M. J. Antarctic basal environment shaped by high-pressure flow through a subglacial river system. *Nat. Geosci.* (2022). doi:10.1038/s41561-022-01059-1
20. Rignot, E. *et al.* Four decades of Antarctic ice sheet mass balance from 1979–2017. *Proc. Natl. Acad. Sci. U. S. A.* **116**, 1095–1103 (2019).

21. Faure, G. & Mensing, T. M. *The Transantarctic Mountains*. *The Transantarctic Mountains* (2011). doi:10.1007/978-90-481-9390-5
22. Piccione, G. *et al.* Subglacial Precipitates Record East Antarctic Ice Sheet Response To Pleistocene Climate Cycles. *Nat. Commun.* **13**, 1–14 (2022).
23. Sürmelihindi, G. *et al.* Laminated carbonate deposits in Roman aqueducts: Origin, processes and implications. *Sedimentology* **60**, 961–982 (2013).
24. Wróblewski, W., Gradziński, M., Motyka, J. & Stankovič, J. Recently growing subaqueous flowstones: Occurrence, petrography, and growth conditions. *Quat. Int.* **437**, 84–97 (2017).
25. Keller, B. A Bayesian framework for integrated eruption age and age-depth modelling. (2018). doi:doi:10.17605/OSF.IO/TQX3F
26. Hallet, B. Deposits Formed by Subglacial Precipitation of CaCO3. *Geol. Soc. Am. Bull.* **87**, 1003–1015 (1976).
27. Blackburn, T. *et al.* Ice retreat in Wilkes Basin of East Antarctica during a warm interglacial. *Nature* **583**, 554–559 (2020).
28. Miller, E. K., Blum, J. D. & Friedland, A. J. Determination of soil exchangable-cation loss and weathering rates using Sr isotopes. *Nature* **362**, 3–6 (1993).
29. Aciego, S., Bourdon, B., Schwander, J., Baur, H. & Forieri, A. Toward a radiometric ice clock: Uranium ages of the Dome C ice core. *Quat. Sci. Rev.* **30**, 2389–2397 (2011).
30. Andersen, M. B., Erel, Y. & Bourdon, B. Experimental evidence for 234U-238U fractionation during granite weathering with implications for 234U/238U in natural waters. *Geochim. Cosmochim. Acta* **73**, 4124–4141 (2009).
31. Anderson, H. J., Pedro, J. B., Bostock, H. C., Chase, Z. & Noble, T. L. Compiled Southern Ocean sea surface temperatures correlate with Antarctic Isotope Maxima. *Quat. Sci. Rev.* **255**, 106821 (2021).
32. Crowley, T. J. North Atlantic Deep Water Cools the Southern Hemisphere. *Paleoceanography* **7**, 489–497 (1992).
33. Lee, S. Y., Chiang, J. C. H., Matsumoto, K. & Tokos, K. S. Southern Ocean wind response to North Atlantic cooling and the rise in atmospheric CO2: Modeling perspective and paleoceanographic implications. *Paleoceanography* **26**, 1–16 (2011).
34. Barker, S. & Knorr, G. Millennial scale feedbacks determine the shape and rapidity of glacial termination. *Nat. Commun.* **12**, (2021).
35. Members, W. D. P. Precise interpolar phasing of abrupt climate change during the last ice age. *Nature* **520**, 661–665 (2015).
36. Chen, S. *et al.* Strong coupling of Asian Monsoon and Antarctic climates on sub-orbital timescales. *Sci. Rep.* **6**, 1–7 (2016).
37. Joughin, I., Alley, R. B. & Holland, D. M. Ice-Sheet Response to Oceanic Forcing. *Science (80-.).* **338**, 1172–6 (2013).
38. Bell, R. E., Studinger, M., Shuman, C. A., Fahnestock, M. A. & Joughin, I. Large subglacial lakes in East Antarctica at the onset of fast-flowing ice streams. *Nature* **445**, 904–907 (2007).
39. Li, M., Hinnov, L. & Kump, L. Acycle: Time-series analysis software for paleoclimate research and education. *Comput. Geosci.* **127**, 12–22 (2019).
40. Coplen, T. B. *et al.* New Guidelines for δ13C Measurements. *Anal. Chem.* **78**, 2439–2441 (2006).
41. Ostermann, D. R. & Curry, W. B. Calibration of stable isotopic data: An enriched δ18O

standard used for source gas mixing detection and correction. *Paleoceanography* **15**, 353–360 (2000).
42. Lisiecki, L. E. & Raymo, M. E. A Pliocene-Pleistocene stack of 57 globally distributed benthic δ 18O records. *Paleoceanography* **20**, 1–17 (2005).

FIGURES:

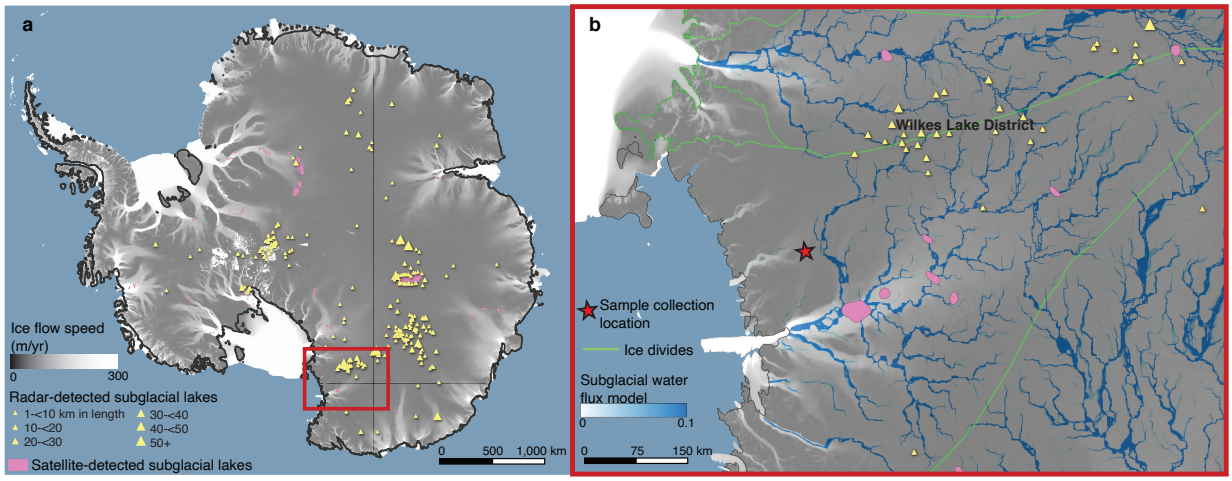

Figure 1 | Map of Antarctic Subglacial Lakes. a. Map of the Antarctica ice velocity (black-white gradient) showing radar (yellow) and satellite detected (pink) subglacial lakes. The boxed area of the East Antarctic Ice Sheet (EAIS) is the Mawson glacier catchment, shown in panel (b). **b.** Map of subglacial water from inset in panel (a). Subglacial lakes from the Wilkes lakes region (yellow diamonds) are located upstream of where samples were collected from Reckling Moraine (red star) and are possible lakes contributing to the fill and flush cycles recorded by precipitate samples.

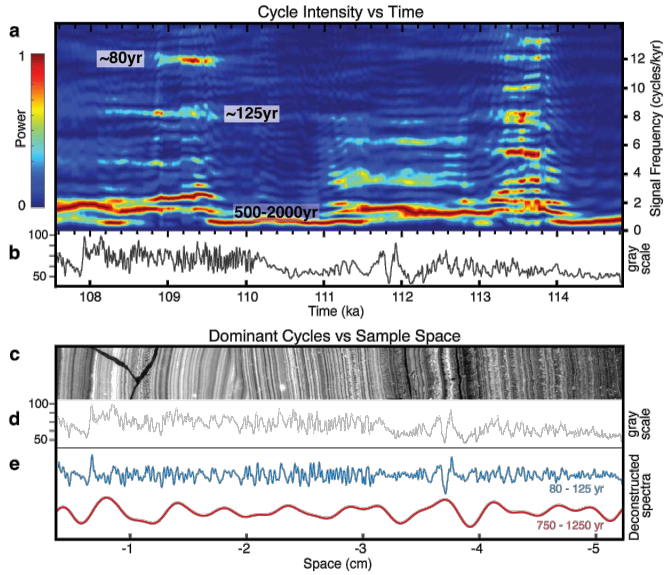

Figure 2 | Spectral Analyses of sample PRR53557. a. Evolutionary FFT analysis of detrital silicate concentration showing cycle power over time. **b.** Spectral data derived from calcite opacity of sample thin section plotted in the time domain. **c.** grey scale image of sample. **d.** Spectral data in space domain. **e.** deconstructed spectra for centennial scale (blue) and millennial scale (red) cyclicity in sediment (Methods). A complementary figure for sample PRR52588 is included in the extended data (Extended Data Fig. 4).

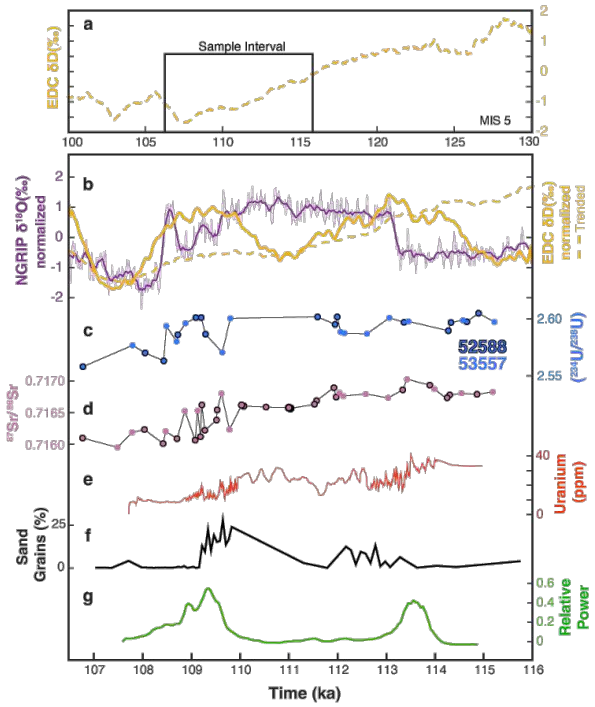

Figure 3 | Comparison between sample PRR53557 and climate records. **a.** δD (‰) a proxy for Antarctic surface temperature at EPICA Dome C (EDC), on the AICC2012 timescale, over the last interglacial. **b.** (Dashed yellow) EDC δD (‰) over sample interval (box inset from panel a). (Purple) Northern Greenland Ice Core Project δ^{18}O (‰) record, a proxy for temperature in Greenland showing polar seesaw related Dansgaard-Oeschger (D-O) events at ~109 and 113 ka. (Solid yellow) decomposed AIMs from EDC by removal of the LR04 marine isotope record[42] following[36]. b-e) Measured geochemical data from subglacial precipitates. f) abundance sand grains (measured in percent of total sample area). g) spectral power through time of periodicities from 80 – 130 yr.

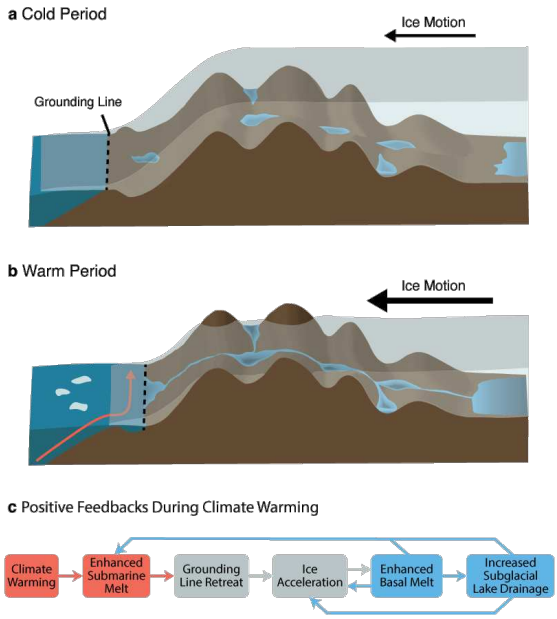

Figure 4 | Schematic illustration of the EAIS differing under Southern Ocean temperature conditions. a. Cold period conditions result in an advanced grounding line, thicker ice shelf, and subglacial hydrologic system isolated by regions of basal freezing. **b.** Warmer ocean conditions cause grounding line retreat, ice acceleration and thinning, and a response from the hydrologic system that includes increased water volumes and connectivity to interior lakes with longer rock-water interaction times. **c.** Proposed positive feedback between climate, subglacial hydrology and ice loss. Red boxes pertain to climate forcing, gray to the ice response and blue to subglacial hydrology.

Supplementary Files

This is a list of supplementary files associated with this preprint. Click to download.

- ExtendedDataFigures.pdf
- ExtendedDataTable1UTH.xlsx
- ExtendedDataTable2StableIC.xlsx
- ExtendedDataTable3Sr.xlsx